Materials Today Chemistry 26 (2022) 101044

Contents lists available at ScienceDirect

Materials Today Chemistry

journal homepage: www.journals.elsevier.com/materials-today-chemistry/

An ultrasonic-assisted rapid approach for sustainable fabrication of antibacterial and anti-biofouling membranes via metal-organic frameworks

E. Zolghadr [a, b], M. Dadashi Firouzjaei [b, *], S. Aghapour Aktij [c, d], A. Aghaei [c], E.K. Wujcik [e], M. Sadrzadeh [c], A. Rahimpour [c], F.A. Afkhami [f], P. LeClair [a], M. Elliott [b, **]

[a] Department of Physics and Astronomy, University of Alabama, Tuscaloosa, AL, 35487, USA
[b] Department of Civil, Construction and Environmental Engineering, University of Alabama, Tuscaloosa, AL, 35487, USA
[c] Department of Mechanical Engineering, 10-367 Donadeo Innovation Center for Engineering, Advanced Water Research Lab (AWRL), University of Alberta, Edmonton, AB, T6G 1H9, Canada
[d] Department of Chemical & Materials Engineering, University of Alberta, Edmonton, AB T6G 1H9, Canada
[e] Department of Chemical and Biological Engineering, University of Alabama, Tuscaloosa, AL, 35487, USA
[f] Department of Chemistry and Biochemistry, University of Alabama, Tuscaloosa, AL, 35487, USA

ARTICLE INFO

Article history:
Received 17 March 2022
Received in revised form
10 June 2022
Accepted 13 June 2022
Available online 18 July 2022

Keywords:
Surface modification
Antibacterial activities
Biofouling
Microfiltration
Ultrasonication
Green chemistry
MOF

ABSTRACT

Biofouling is a pivotal problem for polymeric membranes used in water treatment and reuse. Surface functionalization is a promising practice to improve the resistance of membranes to biofouling. Diverse materials, synthesis methods, and functionalization techniques will be needed to address different applications. Herein, we employed a novel ultrasonic-assisted technique to functionalize polyvinylidene fluoride microfiltration membranes by silver-based metal-organic frameworks (AgMOFs). Polydopamine (PDA) coating was also used to carry out this surface modification. In this study, AgMOFs were synthesized and in-situ grafted on the membrane surface simultaneously using ultrasonication for the first time. Unlike the conventional methods in which AgMOFs are prone to be washed away, the AgMOFs synthesized by ultrasonic-assisted method strongly bonded with the PDA-coated membrane. In addition, the MOF-PDA membrane fabricated by this method showed more uniform and size-controlled AgMOFs on the membrane surface than other conventional methods with large MOF clusters. The AgMOF-functionalized membrane displayed enhanced static antibacterial activity and dynamic biofouling resistance compared to those of the PDA-coated and pristine membranes while in contact with the model bacteria, *Escherichia coli* and *Staphylococcus aureus*. These results were evidenced by a larger inhibition zone area, a decline in viable cells observed in static antibacterial experiments, and more retained water flux in dynamic biofouling experiments. Altogether, our findings indicate that the in-situ synthesis of AgMOFs on membrane surfaces was successful by this facile and environmentally friendly method which can be considered in future studies with the purpose of surface modification for diverse applications.

1. Introduction

Microfiltration is a low-pressure membrane process often used for removing suspended solids, especially bacteria, from wastewater [1–3]. It is considered one of the most effective methods to pretreat the wastewater prior to post-treatment methods such as reverse osmosis and ultraviolet disinfection [4,5]. However, numerous challenges associated with microorganisms in the feed, including bacterial attachment, colonization, and eventually biofilm formation on the membrane surface, hinder the widespread application of microfiltration for bacteria removal [6]. Biofouling, as the 'Achilles' heel' of membrane processes [7,8], not only microfiltration, leads to adverse impacts on membrane water flux, lifespan, and overall operation cost [9,10]. Moreover, metabolic

* Corresponding author.
** Corresponding author.
E-mail addresses: mdfirouzjaei@crimson.ua.edu (M. Dadashi Firouzjaei), melliott@eng.ua.edu (M. Elliott).

https://doi.org/10.1016/j.mtchem.2022.101044
2468-5194/

products generated by bacteria on the membrane surface can penetrate the permeate and cause secondary contamination of water, putting human health in danger [11]. Despite many past studies on biofouling control strategies, a robust solution for preventing biofilm formation in membrane-based treatments is still elusive [12,13]. Therefore, novel approaches to mitigate biofouling are of huge importance.

Past efforts to mitigate biofouling are mostly biological-based control methods (for instance, quorum quenching [14]) and surface modification of the membranes [15]. The latter has attracted significant attention in the last decade due to its high efficiency in biofouling mitigation, low cost, and versatility [16,17]. Numerous surface functionalization strategies have been investigated to avoid bacterial adhesion to the membrane surface through tuning surface roughness [18], hydrophilicity [19,20], and charge [21,22]. Despite successful results at the initial stage, these strategies 'could not control biofouling in long-term operations as it only takes a few bacterial cells attached to the membrane surface to form a biofilm [23]. Some other studies focused on grafting biocidal agents, e.g. silver [24] and copper [25,26] nanoparticles, on the membrane surface to attack and inactivate bacteria by releasing ions. While grafting such nanomaterials was found to be effective in lab-scale and short-term operations, the fabricated membranes suffer from low robustness due to the loss of antibacterial activity over time [27]. In addition, this method requires a relatively large load of nanoparticles to keep up with an efficient release, which not only increases the fabrication cost but also potentially causes negative impacts on human health and the environment [28]. On the other hand, metal-organic frameworks (MOFs), as emerging high-performance porous materials with antimicrobial properties, can be used as a reservoir of uniformly distributed biocidal metal ions on a membrane surface, in which the continuous gradual release of the metal ions by (bio)degradation of the framework provides sustainable antibacterial activity [29–31]. The key advantages of MOFs over other materials loaded with metal ions are (1) sustained release capability, (2) accommodating porosity, (3) uniform distribution of the active metal sites, and (4) structural tunability by using different metals and/or organic ligands [32,33]. Furthermore, the organic ligands used to fabricate MOFs may offer additional antimicrobial properties. The spatial structure of MOFs can store ligand molecules so that the antimicrobial activities of the metal ions and the organic ligand can be combined [32,34,35].

In addition, in-situ growth of MOFs on the membrane surface can substantially improve membrane performance by changing the surface's roughness, wettability, and charge. Liu et al. [36] showed that coating the polyethersulfone (PES) substrate with UiO-66 MOF led to a flux recovery rate higher than 95%. Xu et al. [37] indicated that in-situ growth of zeolite imidazolate frameworks-8 (ZIF-8) on the PES substrate using dip-coating improved both water permeance and salt rejection. Zhang et al. [38] modified the surface of polyamide (PA) substrate by in-situ conversion of ZnO into ZIF-8, resulting in better dispersion of ZIF-8 on the membrane surface. Li et al. [39] achieved a rejection higher than 99.5% for Congo Red and Rose Bengal sodium salt through in-situ growth of UiO-66-NH_2 MOFs on the PES membrane surface.

Among MOFs, silver-based MOFs (AgMOFs) attracted significant attention in the literature for water treatment applications [30,40–42]. Nevertheless, most of these studies have demonstrated moderate improvements in bacterial inactivation and overcoming biofilm formation. Moreover, the approaches used in previous studies for synthesis and grafting MOFs on the membrane surface are complex and energy- and cost-intensive [43–45]. MOFs are typically synthesized in a solvent and at temperatures ranging from room temperature to nearly 250 °C [46]. The required energy is generally introduced through various means, such as conventional electric heating, microwave heating, mechanochemistry, electrochemistry, and sonochemistry (ultrasonic) methods [43,47–49], among which sonochemistry is found to be the most advantageous in terms of energy efficiency and environmental friendliness [50]. Sonochemistry has been widely used before in synthesizing organic materials [51] and nanomaterials [52,53]. It was employed for the first time to synthesize MOFs in 2008 [46,54]. The rapid, low-temperature sonochemical synthesis of MOFs inspired us to develop a facile and scalable approach for the surface modification of water purification membranes.

In this work, AgMOF was in-situ grown on the surface of microfiltration polymeric membranes using ultrasonication. Using the polydopamine' functionality [55], AgMOF was grafted on the surface of microfiltration polyvinylidene fluoride (PVDF) membranes through two separate steps: (1) PDA surface coating and (2) in-situ AgMOF immobilization. This approach results in a firm attachment of AgMOF to the surface of the PDA-coated membrane. The synthesized membranes were extensively characterized to confirm the successful grafting of AgMOFs to the membrane surface. We also evaluated the antibacterial behavior of the AgMOF-decorated membranes through different static antibacterial tests, including disc inhibition zone, confocal microscopy, and colony counting tests. Moreover, dynamic biofouling filtration experiments were conducted to validate the improved performance of the modified membranes in terms of permeation properties. To the best of our knowledge, this is the first work to employ ultrasonic-assisted in-situ grafting to incorporate the AgMOF biocidal agents onto a membrane surface.

2. Materials and methods

2.1. Materials and chemicals

A commercial PVDF microfiltration membrane (Durapore Membrane Filter, MilliporeSigma Inc.) with a nominal pore size of 0.22 μm and an average thickness of 110 μm was used substrate for surface modification. Silver nitrate ($AgNO_3$), benzene-1,3,5-tricarboxylic acid (trimesic acid), dopamine hydrochloride, and tris(hydroxymethyl) aminomethane (Tris) were supplied by Sigma-Aldrich.

2.2. Surface modification of membranes by PDA

The pristine PVDF membrane (Blank membrane) was first dip-coated by the dopamine monomer via immersing in 100 mL of dopamine (2 g/L) -Tris (25 mM, pH 8.5) solution and shaking at 37 °C [56] for 24 h during which the self-polymerization of dopamine occurs. Then, the remaining dopamine-Tris solution was discarded, and the membrane was carefully rinsed with deionized (DI) water and dried before further modification. The resulting PDA-coated membrane was denoted as PDA membrane.

2.3. In-situ growth of AgMOF on membrane

$AgNO_3$ as a metal source and trimesic acid as an organic ligand were used to synthesize AgMOFs. 1 g of $AgNO_3$ and trimesic acid were, respectively, dissolved in 40 mL DI water and ethanol to prepare metal and ligand solutions. Next, the two solutions were slowly stirred at 100 rpm for 20 min. The solutions were then slowly poured on top of the PDA membrane, which was mounted in a lab-made frame, all settled at the bottom of a container. After that, the ultrasonication was carried out using a probe sonicator (Q500 Sonicator, Qsonica, USA) at the optimized condition of 5 s pulse-pause time with a total duration of 1 h (Fig. S1). Water was used as an external coolant to regulate the temperature and avoid the

fast evaporation of the solution during ultrasonication. The temperature of the mixed solution was also monitored throughout the ultrasonication time by a thermometer (Fig. S2). After the ultrasonication was over, the membrane was thoroughly rinsed with DI water to detach unreacted AgMOFs. The functionalized membrane is referred to as the MOF-PDA membrane. Fig. 1 schematically shows the fabrication process and the surface chemistry of the membranes. It should be noted that in the conventional method, the AgMOF nanoparticles are pre-synthesized, and the AgMOF solution is poured on a substrate. The main restriction of this method is that the AgMOF nanoparticles do not react with the PDA-coated surface and are easily washed away when rinsing with DI water during the surface modification or the filtration process. A similar fabrication process was carried out to in-situ graft AgMOFs on the non-coated PVDF substrate. However, the AgMOFs could not efficiently react with the PVDF substrate and were quickly washed away. Therefore, the performance of the PVDF-AgMOF membrane was not evaluated in this work.

2.4. Membrane characterization

The surface morphology of the membranes was observed using scanning electron microscopy (SEM; Apreo Thermo Fisher Scientific, USA) after coating with a 5-nm-thick layer of gold on the membranes using a sputter coater (Leica EM ACE600, USA). Transmission electron microscopy (TEM; FEI Tecnai F-20, USA) was also employed for further investigation. Atomic force microscopy (AFM; EasyScan II, Switzerland) was employed to investigate the surface roughness of the membranes, providing estimates of different parameters, including arithmetic average roughness (R_a) and root mean square average roughness (R_q).

The elemental composition and functional groups of the membranes were investigated by X-ray photoelectron spectroscopy (XPS) performed using a Kratos spectrometer (Axis 165 XPS/Auger, Shimadzu, Japan) equipped with a 100 μm monochromatic Al K (alpha) X-ray. Furthermore, the chemical properties of the membrane surfaces were further investigated using attenuated total reflection-Fourier transform infrared (ATR-FTIR; Nicolet iS50 FT, Thermo Fisher Scientific, USA) and Raman spectroscopies (532 nm wavelength coupled to a 10 × objective, OPUS MPC 6000, Laser Quantum). The crystalline patterns of grafted AgMOF particles were identified using X-ray powder diffraction (XRD; Bruker D8, Germany). The operation of mentioned characterization items can be found in other studies [22,57–59].

2.5. Evaluating the antimicrobial activity of membranes

Escherichia coli (*E. coli*) and *Staphylococcus aureus* (*S. aureus*) bacteria, respectively, as model gram-negative and gram-positive bacteria, were used to evaluate the antimicrobial properties of the membranes via a combination of different techniques, including colony-forming units (CFUs) enumeration, confocal laser scanning microscopy (CLSM), and disc inhibition zone tests. Bacteria were cultivated overnight in trypticase soy broth (TSB) at 37 °C with incubation and shaking. The bacteria suspension (1 mL) was transferred to fresh TSB media (9 mL) and grown for ~4 h until it reached an optical density of 1.4 at 600-nm wavelength. The cells were centrifuged for 10 min at 10,000 g (Multifuge X1R Centrifuge, Thermo Fisher Scientific, USA), washed with phosphate-buffered saline solution, and then diluted to 10^7 CFU/mL for CFU enumeration and CLSM tests and to 10^6 CFU/mL for disc inhibition zone test.

CFU enumeration tests were performed using an assay described in previous studies [27,60]. Circular membrane coupons with an area of ~2 cm^2 (a diameter of 15.9 mm) were cut and placed in contact with the bacterial suspension (10 mL) for 1 h. After incubation, the bacterial suspensions were discarded, and the membrane coupons were transferred into fresh tubes containing 10 mL of phosphate-buffered saline. Then the tubes were bath-sonicated for 5 min to have deposited bacteria detached from the surface of membranes. The resulted suspensions were mixed and then plated (pipetted 0.1 mL onto the surface of solidified TSB agar plates and slowly spread) and incubated overnight at 37 °C for 24 h. Following incubation, the colonies were counted to quantify the number of viable cells on the MOF-PDA membrane compared to that on the PDA and Blank membranes.

The antibacterial activity of the membranes was further examined by the CLSM test, for which a live/dead fluorescent staining assay (BacLight bacterial viability kit) was used to determine the viability of bacterial cells on the surface of the membranes [60,61]. Briefly, membranes were placed in contact with *E. coli* or *S. aureus* suspension for 15 min, after which surface-attached bacteria were stained with propidium iodide (PI) and SYTO 9 for staining dead and live cells, respectively. Then, a confocal laser scanning microscope (C2, Nikon Corporation, Japan) was employed to take images

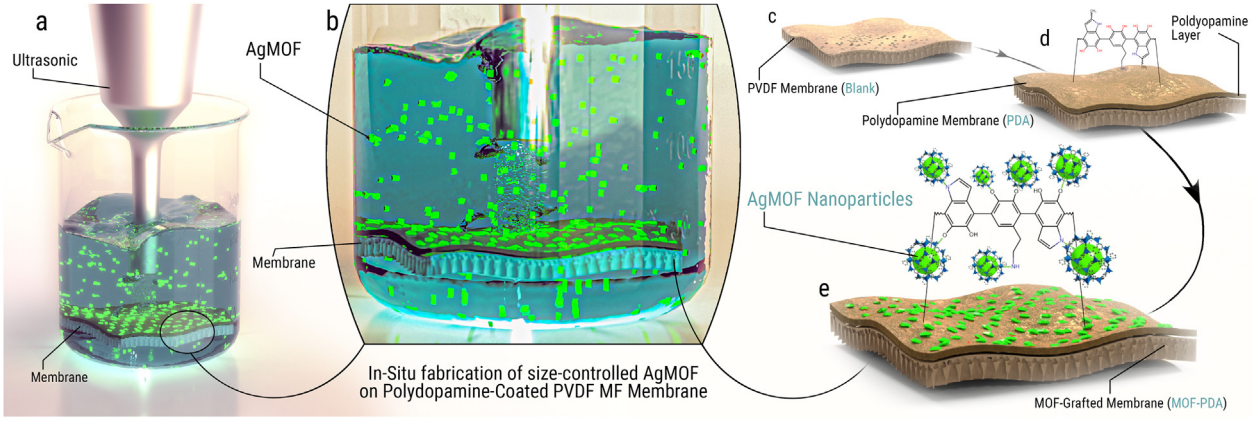

Fig. 1. Schematic illustration of membranes surface modification. (**a**) Ultrasonic fabrication of AgMOFs on PDA membrane. Herein, the AgMOFs were in-situ fabricated on the PDA membrane surface and resulted in the MOF-PDA membranes. (**b**) The magnified snapshot of the ultrasonic process. The residue, or by-product of AgMOF nanoparticles, is floating in an $AgNO_3$-trimesic solution. The by-product AgMOFs were collected and used for antibacterial applications to show the efficiency of the process. This novel membrane modification approach shortens the fabrication process and increases efficiency. The MOF-PDA membranes possess more uniform and size-controlled AgMOFs than conventional methods with large MOF clusters. (**c**) PVDF pristine membrane denoted as Blank membrane. (**d**) Polydopamine-coated membrane denoted as PDA membrane. (**e**) AgMOF-functionalized membrane denoted as MOF-PDA membrane. MOF, metal-organic framework; PDA, polydopamine; PVDF, polyvinylidene fluoride.

of the samples. The images were analyzed using ImageJ to count the number of bacteria stained with PI or SYTO 9. The following equation calculated the inhibition rate to compare the antibacterial activity of different membranes:

$$\text{Inhibition Rate} = \frac{\text{Total number of dead bacteria}}{\text{Total number of bacteria}} \quad (1)$$

To further investigate the antimicrobial activity of the membranes, a disc inhibition zone test was performed to identify and compare the inhibition zone of pristine and modified membranes. First, TSB agar plates were poured and allowed to solidify in a biosafety cabinet. The plates were exposed to ultraviolet light for a few minutes to eliminate contamination. *E. coli* and *S. aureus* fresh suspensions were obtained as described above. Subsequently, a sterile cotton swab was dipped into the *E. coli* or *S. aureus* suspension and uniformly spread on the TSB agar plates. Membrane discs with a diameter of 15.9 mm were placed in the Petri dishes (100 mm diameter), exposing the active surface side to bacteria. The plates were then incubated and monitored for ~12 h at 37 °C. Finally, photos of the Petri dishes and detected inhibited zone of the membranes were taken using a digital camera (EOS 1200D, Canon, Japan).

2.6. Evaluating the antimicrobial properties of by-Product nanoparticles

The antibacterial activity of by-product AgMOF nanoparticles was evaluated using the paper disc assay [62]. TSB agar plates were prepared with the same procedure as the inhibition zone test for the membranes, using a sterile cotton swab to inoculate the *E. coli* or *S. aureus* bacteria from 10^6 CFU/mL suspensions. On the other hand, different concentrations of AgMOF solution were prepared by dissolving produced AgMOF powder in DI water and serial dilution. Sterile paper discs with a diameter of 6 mm were dipped in 10 mL of AgMOF solution (1 mg/mL). Then, the paper discs were placed in the plates spread with bacteria. Paper discs immersed only in DI water were used as a control. The plates were then incubated and monitored for ~12 h at 37 °C. Finally, photos of the Petri dishes and detected inhibited zones of the discs were taken by a digital camera (EOS 1200D, Canon, Japan).

2.7. Evaluating the anti-biofouling properties

Biofouling experiments were conducted using a dead-end filtration setup. The dead-end cell was customized to fit the circular membranes with a diameter of 47 mm. Before inserting the membrane for each experiment, the whole system, including the membrane cell, feed tank, and pipes, was thoroughly washed using pure ethanol and DI water. A pressurized nitrogen gas tank was employed to apply the pressure. All filtration experiments were carried out with the cell and the feed tank being stirred at 400 rpm. DI water containing model microbes (i.e. *E. coli* or *S. aureus*) was used as a feed solution. An *E. coli* or *S. aureus* suspension (10^9 CFU/mL) was added to the feed to reach ~10^7 CFU/mL initial bacterial concentration. Biofouling experiments were performed at room temperature and ~0.6 bar for 4 h, with water flux monitored at 1 min intervals. The measured water flux (J_w) was obtained using the following equation:

$$J_w = \frac{V}{A \times t} \quad (2)$$

where V is the permeated volume of water (L), A is the area of the membrane (m^2), and t is the operation time (h). The accumulated permeate volume data were collected every minute. The average values and corresponding errors were calculated based on the standard deviation of the mean for each interval of 10 min. All data points were normalized to the initial flux value.

2.8. Release rate of silver ions

The silver ion release from MOF-PDA membranes was assessed via leaching tests to investigate the environmental sustainability, long-term functionality, and chemical stability of surface-modified membranes. Membrane coupons with an area of 6 cm^2 were incubated in 20 mL of DI water and then placed on a shaker (100 rpm). The water was refreshed every 24 h. After collecting all water samples, each sample was acidified by 1% HNO_3 and examined by inductively coupled plasma-optical emission spectrometry (ICP-OES; Thermo iCAP 6300 Duo ICP-OES, Thermo Fisher Scientific, Germany) to measure the concentration of silver in the samples. The leaching tests were conducted for 14 days.

3. Results and discussion

3.1. Membranes physiochemical and morphological characterization

The surface chemistry of the membranes was investigated using attenuated total reflection-Fourier transform infrared spectroscopy (Fig. 2a). The dominant peak at 1173 cm^{-1} is a characteristic of PVDF and is due to the symmetric stretching vibrations of the $-CF_2$ group [63–65]. The vibrational band at 763 cm^{-1} is assigned to in-plane bending in the PVDF α-phase [64,65], and the peak at around 840 cm^{-1} is the characteristic of β-phase [64,66]. Moreover, the bands at 1234 and 1453 cm^{-1} are, respectively, attributed to γ-phase [67] and the in-plane bending of the $-CH_2$ group [64]. Furthermore, the observed peaks at 2980 and 3023 cm^{-1} are associated with the asymmetric and symmetric stretching vibrations of the $-CH_2$ group, respectively [68,69]. Notably, a broad peak centered at around 1604 cm^{-1} appeared in the FTIR spectrum of the PDA membrane; this peak is attributed to the stretching vibration of PDA groups [70]. This peak becomes sharper and shifts to 1609 cm^{-1} in the FTIR spectrum of MOF-PDA. An extra peak at 1566 cm^{-1} also shows up. These changes could be due to the interactions between the AgMOF and PDA [70,71], implying the successful modification of membranes.

Further characterization of the membranes was done by studying the XRD patterns provided in Fig. 2b. The three dominant peaks observed for all membranes at $2\theta = 18.1$, 18.7, and 20.3° are due to the semi-crystalline α-phase structure of PVDF [72], and are, respectively, ascribed to (100), (020), and (110) diffraction indices [73]. Notably, the XRD pattern of the MOF-PDA membrane demonstrates several sharp peaks in the range of 25–38° in addition to one single peak at $2\theta = 16.4°$ that are not observed in the patterns of the Blank and PDA membranes. These peaks are indicative diffraction patterns of AgMOF crystalline structure, among which peaks at $2\theta = 16.4$, and 32.8 represent the (011) and (122) silver crystalline planes, respectively [74–77], which further confirm the presence of AgMOF on the modified surface of MOF-PDA membrane.

Raman spectra of membranes are shown in Fig. 2c. The characteristic Raman modes of PVDF in the Blank membrane spectrum are clearly observed at 795 and 840 cm^{-1}, which are associated with the α-phase and β-phase PVDF, respectively [78,79]. More precisely, the band at 795 cm^{-1} is ascribed to CH_2 rocking mode in α-phase [80], and the band at 840 cm^{-1} is due to the combination of CH_2 rocking mode in β-phase and CF_2 anti-symmetric stretching mode [81]. Moreover, the sharp peak at 1430 cm^{-1} in the Blank membrane spectrum is assigned to CH_2 scissoring and wagging

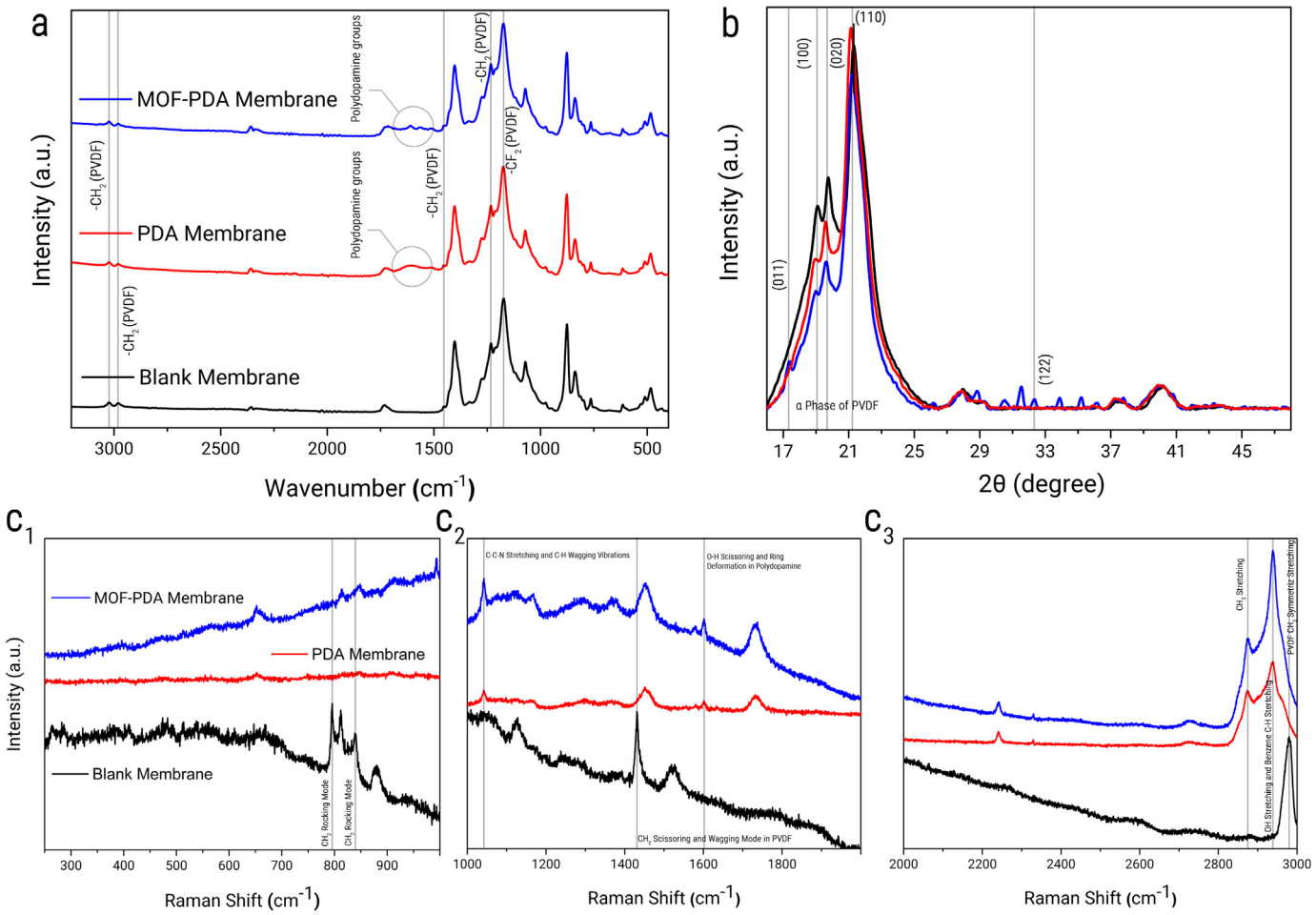

Fig. 2. (**a**) The ATR-FTIR, (**b**) XRD, and (C_1–C_3) Raman spectra of the membranes. The characterization spectroscopy of the membranes shows the successful grafting of AgMOF on the membrane surface. Polydopamine-coating was detected on both PDA and MOF-PDA membranes. The circled FTIR range show the appearance of multiple peaks attributed to polydopamine groups. The extra peaks observed in XRD spectrum of MOF-PDA are due to diffraction patterns of AgMOF crystalline structure. The highlighted Raman peaks represent the vibrational modes in PVDF Blank and modified membranes structure. New vibrational modes and peak shifts due to presence of new functional groups are observed in PDA and MOF-PDA spectra. ATR-FTIR, attenuated total reflection-Fourier transform infrared; MOF, metal-organic framework; PDA, polydopamine; PVDF, polyvinylidene fluoride; XRD, X-ray powder diffraction.

modes in PVDF structure [80]. Compared with the Blank membrane's spectrum, it is notable that the Raman spectra of PDA and MOF-PDA membranes show a few extra peaks. Notably, the peaks observed at 1041 and 1601 cm^{-1} suggest the formation of dopamine; the former is assigned to C–C–N stretching and C–H wagging vibrations, and the latter is associated with O–H scissoring and ring deformation in PDA structure [82]. Moreover, the Raman band at 1452 cm^{-1} corresponds to C–H scissoring [82]. The appearance of two prominent peaks detected at around 2874 and 2938 cm^{-1} for PDA and MOF-PDA membranes also insinuates the successful surface modification. CH_3 stretching vibrations are responsible for the peak at 2874 cm^{-1} [83], and the combination of O–H stretching and benzene C–H stretching modes are associated with the peak at 2938 cm^{-1} [83–85]. Clearly, these peaks did not appear in the Blank membrane as these species are not present in the PVDF structure. Here, the peak at 2980 cm^{-1} coming from PVDF CH_2 symmetric stretching vibrations is still but barely observed at the shoulder of the sharp peak at 2938 cm^{-1}. It is evident that the intensity of the peaks associated with the PVDF structure in the spectrum of the Blank membrane reduces with the surface modification through PDA coating and AgMOF grafting in the spectra of PDA and MOF-PDA membranes. Furthermore, compared with PDA membrane's spectrum, the intensity of new peaks is higher in the MOF-PDA spectrum due to the presence of aromatic benzene ring and O–H bond in the structure of AgMOF ligand as well.

Fig. 3a represents the survey and high-resolution XPS spectra of membranes in which the corresponding peaks for C 1s, F 1s, N 1s, O 1s, and Ag 3 d are marked. As expected, all membranes showed peaks for carbon (C) and fluorine (F), originating from the PVDF structure. Considering the elements and the groups bonded to the carbon atoms, the corresponding peak for C 1s could be deconvoluted into four peaks [86]. Two major Gaussian peaks centered at 285.9 and 290.4 eV in the C 1s spectrum of Blank membrane are ascribed to the contributions of $-CH_2-$ and $-CF_2-$ species [86,87]. Both these peaks, especially the latter, diminished in the spectra of PDA and MOF-PDA membranes as the active surface of the membranes went under modification. The lowest energy peak seen at 284.4 eV is associated with C–H and C–C bonds, which become more dominant in modified membranes [86,88]. Furthermore, the observed peak at 288.3 eV in the spectrum of the Blank membrane is attributed to C=O species, which are most likely caused by the interaction of carbon atoms with electron-withdrawing atoms of oxygen in the environment, usually referred to as adventitious carbon [86,88,89]. This peak might also be due to potential additives in the commercial PVDF membrane [86]. Evidently, this peak becomes more intense in the spectra of PDA and MOF-PDA

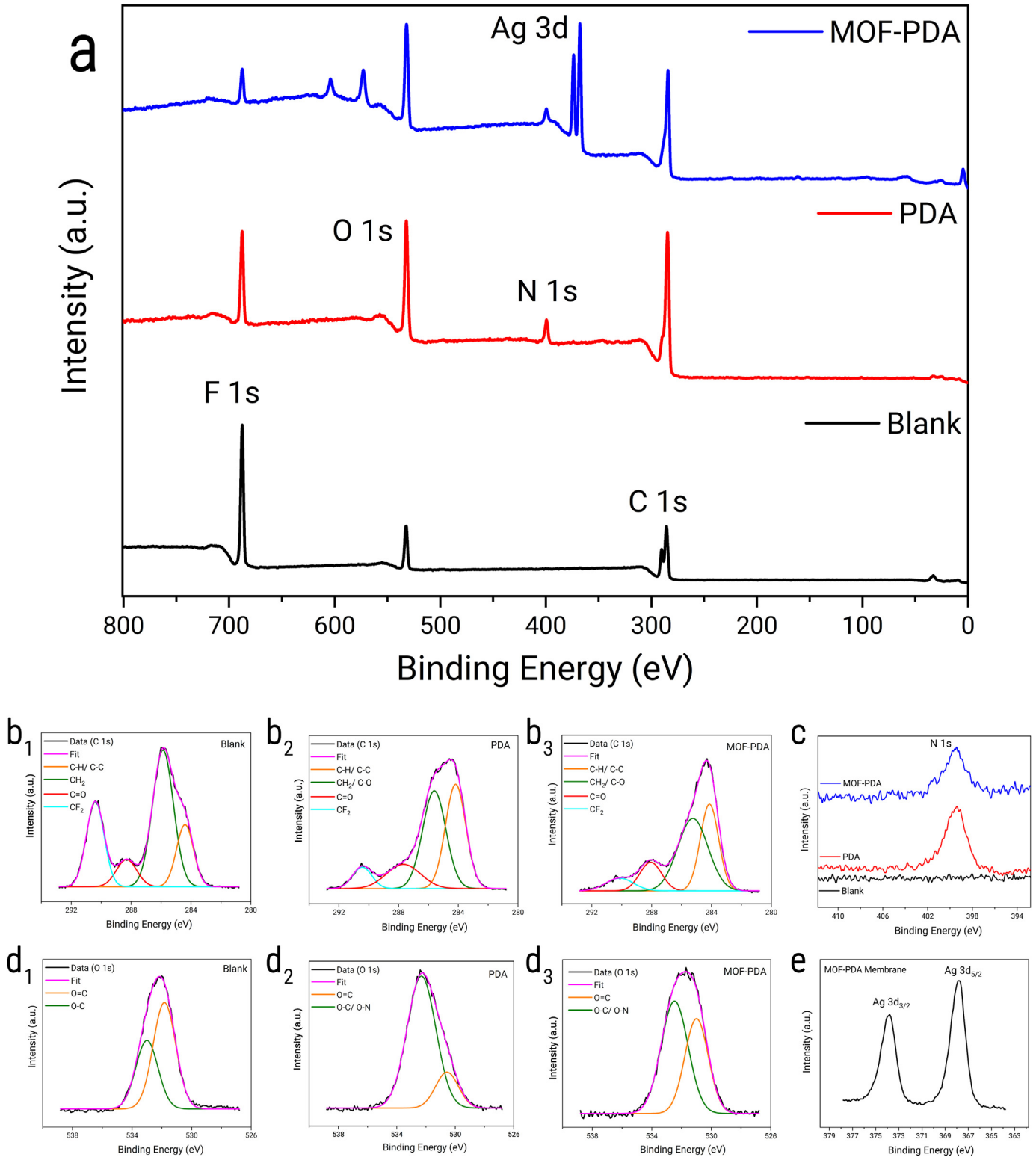

Fig. 3. (**a**) The XPS survey spectra of the membranes, (b–e) the high-resolution deconvoluted XPS spectra of the membranes. The XPS data shows the existence of AgMOF bonds on the surface of the membrane. The two prominent silver signals (Ag $3d_{5/2}$ and $3d_{3/2}$) are observed in the XPS spectrum of MOF-PDA, verifying the existence of AgMOF bonds on the surface of the membrane. In addition, the appearance of nitrogen (N 1s) signal in the XPS spectra of modified membranes also confirms the successful modification of these membranes. MOF, metal-organic framework; PDA, polydopamine; XPS, X-ray photoelectron spectroscopy.

membranes, where more chemical bonds between C and O atoms are involved due to the presence of PDA and AgMOF on the surface.

For the same reasons mentioned above, the corresponding peak of O 1s is observed for the Blank membrane at 532.1 eV [88]. This peak is clearly enhanced in the spectra of modified membranes as more oxygen atoms contribute to the elemental composition of the membranes by having PDA and/or AgMOF on the surface. The corresponding peak of oxygen could also be deconvoluted to two Gaussian peaks at around 531.8 and 533.0 eV, in which the former is responsible for O=C bonds and the latter is assigned to O–Cand O–N (in PDA and MOF-PDA membranes where nitrogen is present) species [41,88,90]. Moreover, the appearance of nitrogen (N1s) signal at about 399.4 eV [40,91] in the XPS spectra of modified membranes also confirms the successful modification of these membranes. In contrast, this signal is not detected for the Blank membrane as there is no nitrogen involved in PVDF structure. Finally, the two prominent silver signals are observed in the XPS spectrum of MOF-PDA. These peaks, centered at about 367.8 and 373.8 eV, assigned to Ag $3d_{5/2}$ and $3d_{3/2}$, respectively, and primarily due to Ag–N bonding [40,67,68], indicate the presence of AgMOF on the surface of MOF-PDA.

The surface morphology of the membranes before and after each modification was investigated using SEM. For comparison, top surface SEM images of membranes are presented in Figs. 4a–c. The Blank membrane showed a typical sponge-like morphology [92,93]. The top-down SEM image of the PDA membrane with slight change compared to the Blank membrane exhibits that PDA coating is formed on the surface of the PVDF substrate (Fig. 4b_{1-2}). Bright spots with crystalline structures can be observed on the surface of the MOF-PDA membrane (Fig. 4c_{1-4}); these spots are associated with the presence of AgMOF clusters, verifying a successful in-situ synthesis and deposition of AgMOFs on the surface. A broader surface view with less magnification (Fig. 4c_1) indicates that AgMOF nanoparticles were uniformly distributed on the membrane surface. The uniformity of these nanoparticles on the surface is an essential factor in the sustainable performance of membrane during filtration operation regarding the anti-biofouling behavior [94]. In addition, results from TEM images (Fig. 4e_{1-3}) clearly show the formed layer of PDA coating on the blank substrate (Fig. 4e_2). The visible dark spots in the TEM image of the MOF-PDA membrane denote the presence of AgMOFs on the membrane surface, with a particle size range of ~10–100 nm. Notably, the AgMOF nanoparticles were also detected beneath the active surface in the MOF-PDA membrane, owing to their penetration through the membrane's pores during in-situ ultrasonic-assisted fabrication. The pore size of the commercial membranes (0.22 μm), which is much larger than the average size of synthesized AgMOF particles, makes it feasible for the MOF particles to be formed and stored inside the pores and valley regions, making these regions a great reservoir of antifouling agents. This is a vital feature when dealing with different (bio)foulants in the feed, especially when pursuing a higher water flux. Because a higher flux across the large pores in porous microfiltration membranes could exert a more significant drag force on the foulants, leading to rapid foulant attachment,

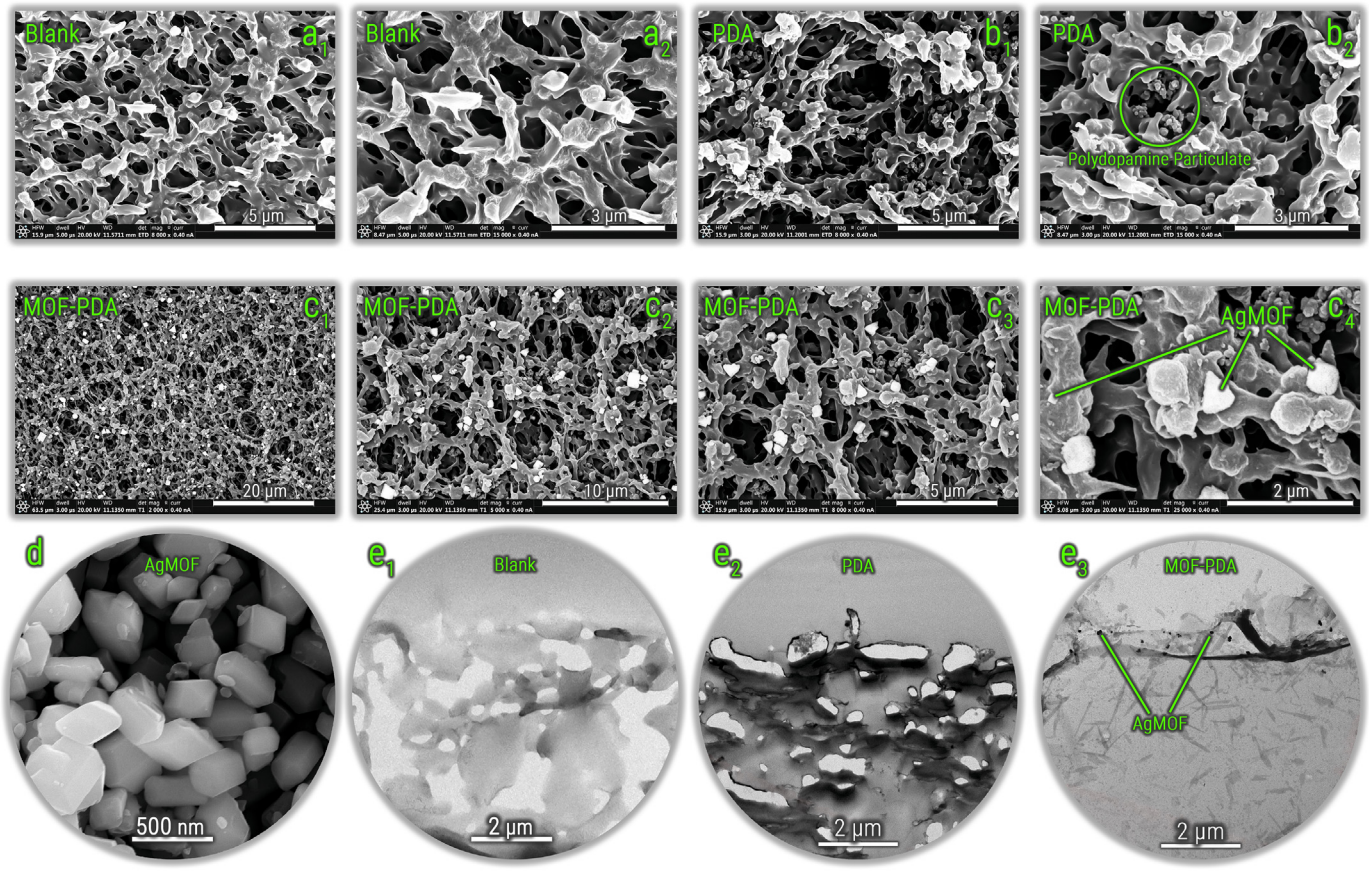

Fig. 4. The SEM images of the (a_1-a_2) Blank, (b_1-b_2) PDA, and (c_1-c_4) MOF-PDA membranes. (d) The SEM image of AgMOF. The TEM images of the (e_1) Blank, (e_2) PDA, and (e_3) MOF-PDA membranes. The MOF-PDA membranes are functionalized with AgMOFs. The SEM and TEM images of the MOF-PDA membrane clearly show that AgMOFs are (I) uniformly distributed, (II) size-controlled, and (III) mainly located on the surface of the MOF-PDA membrane. PDA membrane is coated with polydopamine. The TEM image of the PDA membrane shows darker and thicker layers of PVDF coated with polydopamine compared to the Blank membrane. The particulates of polydopamine are detected in SEM images of the PDA membrane; however, the surface is covered with a thin polydopamine layer. MOF, meta-organic framework; PDA, polydopamine; PVDF, polyvinylidene fluoride.

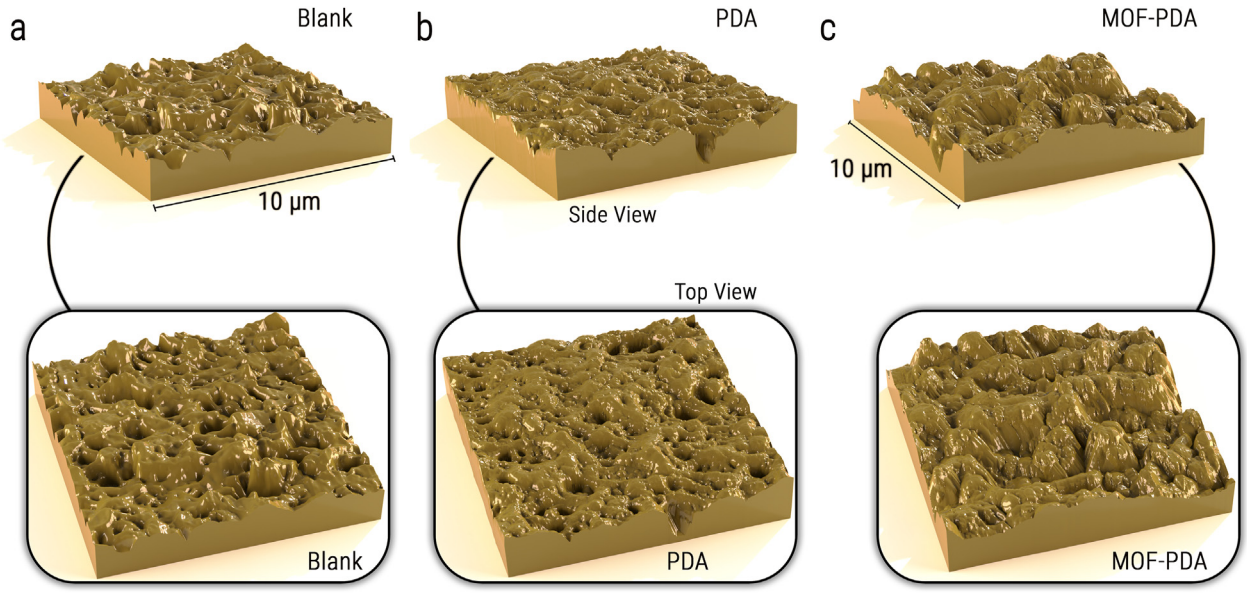

Fig. 5. The side view and top view AFM images of the (**a**) Blank, (**b**) PDA, and (**c**) MOF-PDA membranes. The MOF-PDA membrane is functionalized with AgMOF nanoparticles, agreeing with its higher surface roughness data. However, the MOF-PDA membrane has the lowest surface kurtosis number. AFM, atomic force microscopy; MOF, metal-organic framework; PDA, polydopamine.

which instigates pore blocking and eventually complete fouling [95,96]. Therefore, this is a big advantage for our functionalized membranes and fabrication method to have a sustained high water flux during filtering operation involving microorganisms.

The surface roughness parameters of the membranes before and after functionalization were determined by AFM measurements. Fig. 5 and Table 1**,** respectively, present AFM topographies and the roughness parameters for the membranes. The typical roughness parameters, including root mean square average (R_q), arithmetic average (R_a), and maximum vertical distance (R_{max}), unanimously showed that MOF-PDA has larger roughness values than the other membranes. The grafting of AgMOF nanoparticles on the surface increased the surface roughness in the MOF-PDA membrane, consistent with its SEM and TEM images. Additionally, there is no significant difference in roughness parameters for Blank and PDA membranes which implies that the PDA coating does not substantially alter the surface roughness [97,98]. It has been reported that the membranes with rougher surfaces generally exhibit more tendency toward fouling by macromolecules and bacterial cells [44,99]. However, both PDA and AgMOF contain hydrophilic functional groups such as −OH and −COOH on their structure that improve surface wettability and effectively constrain the foulant adherence, possibly overcoming the adverse effect of roughness on fouling and improving the antifouling behavior [44,98,100]. It is also essential to notice that surface kurtosis (R_{ku}) for the MOF-PDA membrane is less than 3 and smaller than those of Blank and PDA membranes. R_{ku} is a non-dimensional statistical quantity of the surface shape, which describes whether data are distributed flatly or sharply about the central mean [101]. In other words, R_{ku} indicates the sharpness of the height distribution on a surface. It is reported that $R_{ku} < 3$ represents a flat and repetitive surface, while a value larger than 3 suggests a sharper height distribution [102,103]. From AFM analysis, the R_{ku} value is 6.4, 7.8, and 2.7 for the Blank, PDA, and MOF-PDA membranes, respectively. Even though the MOF-PDA membrane possesses a rougher surface based on R_q, R_a, and R_{max}, a smaller R_{ku} value for MOF-PDA may also partially compensate for the adverse effect of roughness on fouling [101].

3.2. Antibacterial and anti-biofouling properties of the membranes

3.2.1. Antibacterial behavior in static contact tests

The antibacterial properties of the membranes were evaluated by different static contact experiments. *E. coli* and *S. aureus* were used in these experiments as model gram-negative and gram-

Table 1
The roughness parameters expressions and their values for the membranes, obtained from AFM measurement analysis.

Roughness parameter	Expression	Membranes		
		Blank	PDA	MOF-PDA
Root mean square average (R_q)	$R_q = \sqrt{\frac{1}{N}\sum_{i=1}^{N} Z_i^2}$	0.16 μm	0.16 μm	0.50 μm
Arithmetic average (R_a)	$R_a = \frac{1}{N}\sum_{i=1}^{N}\lvert Z_i\rvert$	0.12 μm	0.12 μm	0.41 μm
Maximum vertical distance (R_{max})	$R_{max} = Z_{max} - Z_{min}$	1.43 μm	1.45 μm	3.01 μm
Surface kurtosis (R_{ku})	$R_{ku} = \frac{1}{R_q^4} \times \left(\frac{1}{N}\sum_{i=1}^{N} Z_i^4\right)$	6.4	7.8	2.7

Z_i, Z_{max}, and Z_{min}: The height at point i, the maximum Z value, and the minimum Z value, respectivevly
N: Number of points.

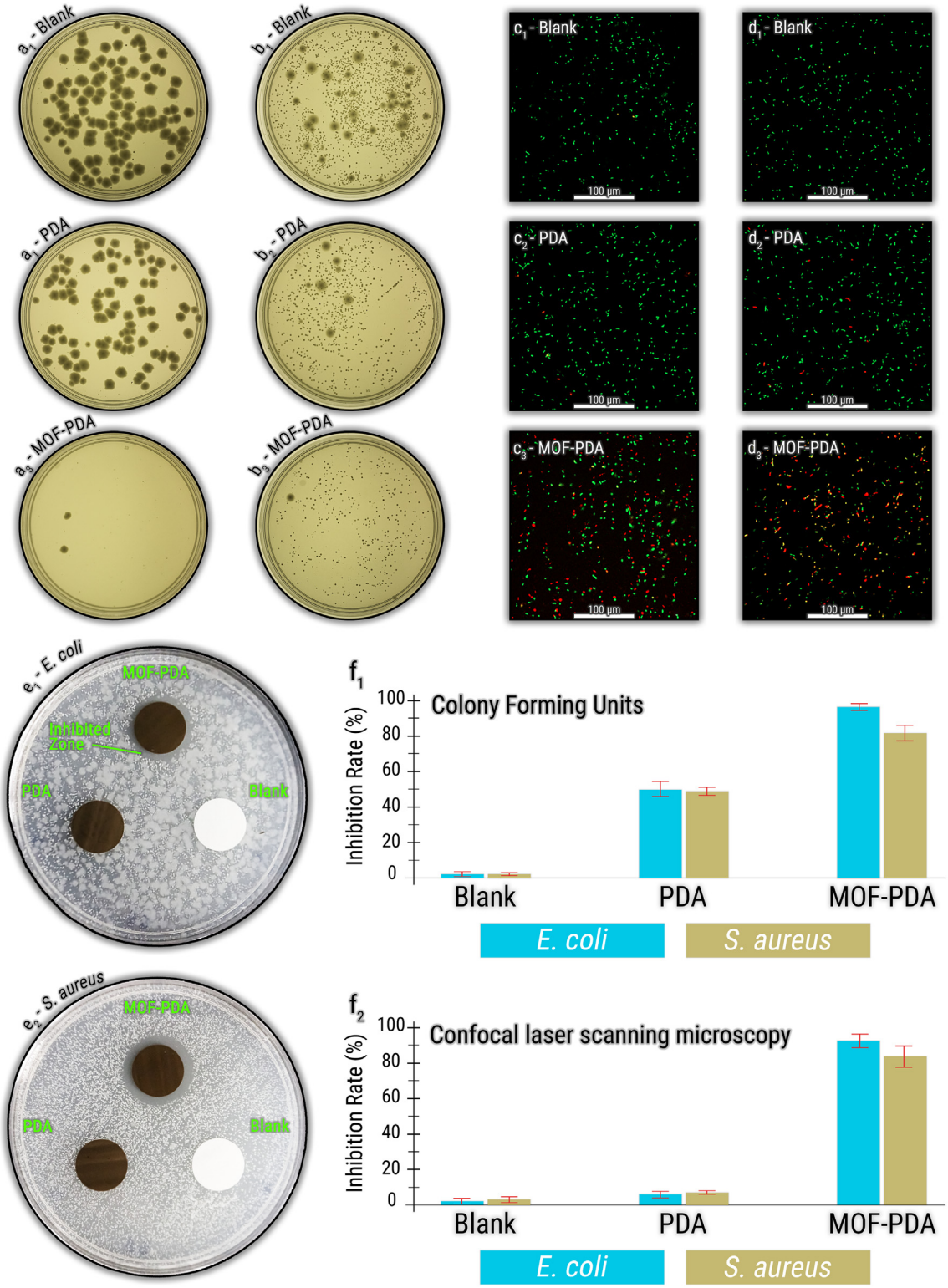

Fig. 6. The antibacterial assessment of the membranes. The colony-forming unit tests membranes against (a_1-a_3) *E. coli* and (b_1-b_3) *S. aureus*. The confocal laser scanning microscopy tests of membranes against (c_1-c_3) *E. coli* and (d_1-d_3) *S. aureus*. The inhibition zone test of membranes against (e_1) *E. coli* and (e_2) *S. aureus*. Bacteria inhibition rates of the membranes in (e) colony-forming unit test and (f) confocal microscopy test.

positive bacteria, respectively. The first experiment was CFUs enumeration, in which membranes were placed in contact with bacterial suspensions, and CFU of bacterial cells attached to the membrane surface were counted. In summary, after the membranes were exposed to *E. coli* or *S. aureus* suspension, bath-sonication was utilized to detach the bacterial cells from the surface; the resulting suspension was mixed, 0.1 mL was plated and plates were counted after overnight incubation. The colonies were counted to quantify the number of viable cells on each membrane. Compared with the Blank membrane, the PDA membrane

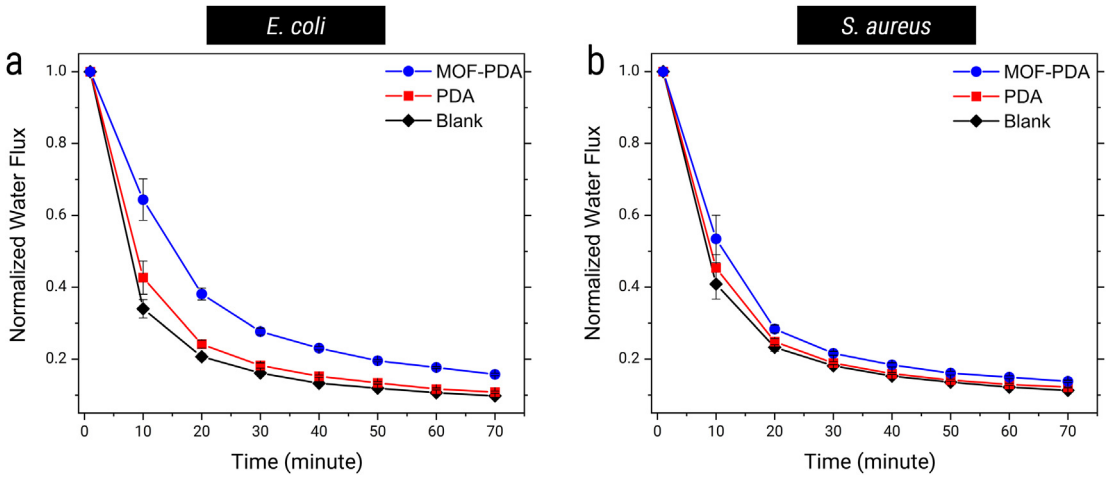

Fig. 7. Water flux of synthesized membranes with (**a**) *E. coli* feed solution and (**b**) *S. aureus* feed solution.

demonstrated ~50% and 49% reduction of viable *E. coli* and *S. aureus* cells, respectively (Fig. 6$a_{1\text{-}2}$ and 6$b_{1\text{-}2}$). The PDA membrane's stronger interaction with bacterial cells in CFU enumeration test than the Blank membrane is caused by altered electrostatic repulsive forces [27,94], most likely due to the hydration layer on PDA coating, which impedes the adhesion of bacterial cells to the surface during this short-time static contact [19,27,104]. The MOF-PDA membrane exhibited improved antibacterial activity with a 97% and 82% CFU reduction for *E. coli* and *S. aureus* cells, respectively (Fig. 6a_3 and 6b_3).

To verify the CFU enumeration test results and further investigate the antibacterial properties of the membranes, we performed a CLSM test, for which a live/dead fluorescent staining assay was used after the membrane surface was exposed to bacterial suspensions. CLSM results revealed that the majority of bacteria (>93%) in contact with the Blank and PDA membrane survived, while a substantial fraction of the cells in contact with MOF-PDA membrane, 93% for *E. coli* and 84% for *S. aureus*, were inactivated. Representative fluorescent images of *E. coli* and *S. aureus* bacteria from the CLSM test for each membrane are provided in Fig. 6c_1-d_3.

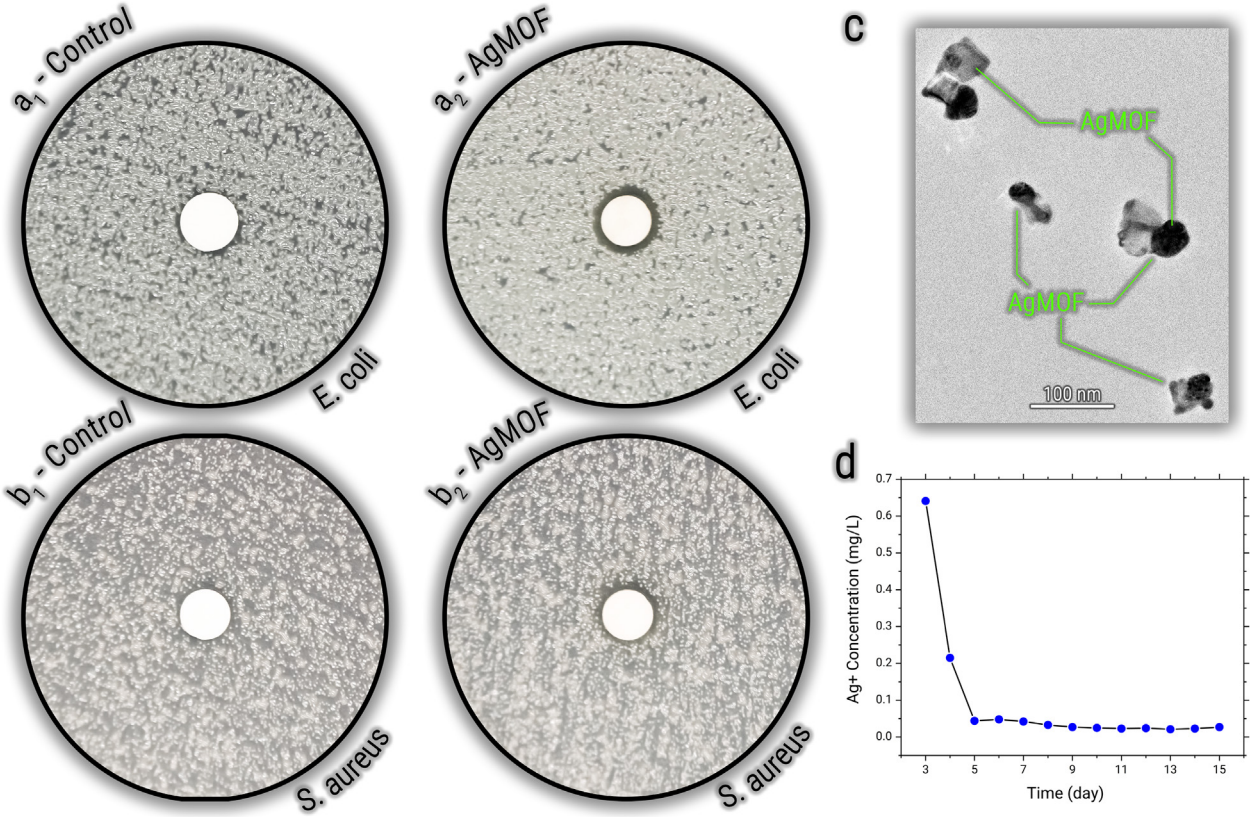

Fig. 8. The sustainability evaluation of the by-product AgMOF and membranes. (**a**), (**b**) The disc inhibition zone test of by-product AgMOF nanoparticles against (**a**) *E. coli*, (**b**) *S. aureus*. (**c**) The TEM image of the by-product AgMOF. (**d**) The silver ion release rate of the functionalized MOF-PDA membrane. MOF, metal-organic framework; PDA, polydopamine; TEM, transmission electron microscopy.

Disc inhibition zone test results yielded similar results. An inhibition zone test can specify the susceptibility of a microorganism to a bactericide material [105]. Fig. 6e$_{1-2}$ illustrates the inhibition zone of *E. coli* and *S. aureus* of the Blank, PDA, and MOF-PDA membranes. No inhibition zone was observed from the Blank and PDA membranes, indicating that these two membranes had no activity against biofilm growth [106]. At the same time, MOF-PDA exhibited superb antibacterial activity to inhibit our model bacteria, showing ~23 mm diameter of inhibited area for both *E. coli* and *S. aureus* biofilms.

The massive death of bacteria could be attributed to AgMOFs on the membrane surface. The gradual release of silver ions with high biocidal properties through (bio)degradation of the employed AgMOFs provides sustainable antibacterial activity. In addition, the organic ligands used in the MOF synthesis donate additional antibacterial properties to the membrane surface. On the other hand, the functional groups of PDA change electrostatic repulsive forces of the membrane surface, resulting in higher antifouling properties.

3.2.2. Anti-biofouling performance in dynamic biofouling experiments

To assess the biofouling resistance of the AgMOF-functionalized membranes and compare it with the Blank membrane, dynamic biofouling experiments were performed using our model bacteria (*E. coli* or *S. aureus*). The initial bacterial concentration was chosen to be relatively high (~10^7 CFU/mL) to have the biofouling process occur faster and distinguish the different performances of the membranes with a restricted volume of feed in a relatively short-time. Fig. 7 presents the water flux during the first 70 min of filtration for membranes with an interval of 10 min. During the filtration experiment, the observed decay in water flux was because of biofilm accumulation on the membrane surfaces. The presence of bacteria in the feed caused a significant decline in the water flux through the Blank membrane, even in the very first minutes of the experiments. On the other hand, the flux decline in MOF-PDA was relatively lower, showing ~66% higher flux than that of Blank membrane after 1 h filtration where the feed solution contained *E. coli*, signifying that MOF-PDA membrane demonstrated enhanced resistance to *E. coli* biofouling compared to the pristine Blank membrane. Our analysis from long-range data suggests that this resistance can be decently sustained for longer times as well, showing ~54% and ~31% higher flux than that of the Blank membrane after 2 and 4 h filtration, respectively (Fig. S3). PDA membrane also exhibited a slightly better performance against *E. coli* biofouling, showing ~10% higher flux than that of the Blank membrane after 1 h filtration due to minor antimicrobial properties of PDA coating on the active surface. This observation is consistent with our results from static antibacterial tests.

Results from filtration of the feed containing *S. aureus* also showed that there is an improved resistance against *S. aureus* biofilm formation in MOF-PDA membrane; however, this behavior is not as promising as anti-biofouling activity against *E. coli*. Only ~23% higher flux than that of the Blank membrane was observed after 1 h filtration with *S. aureus*. This result can be attributed to these two model bacteria's different surface charges and shapes. It is known that *E. coli* has a more negatively charged surface than that of *S. aureus* [107], causing a more repulsive force when interacting with a negatively charged surface of a membrane. In addition, the spherical shape of *S. aureus* with smaller dimensions and a less rigid surface [107–109], in comparison with *E. coli*, makes it more capable of penetrating through the pores of microfiltration membranes and increasing the chance of pore blocking. The better antibacterial performance toward *E. coli* is also consistent with the results from static CFU enumeration and CLSM tests where less resistance was observed against *S. aureus* than *E. coli*. Overall, these results indicate that the AgMOF-functionalized membrane, with a reservoir of biocidal agents on the surface, could delay the biofilm growth by mitigating the initial attachment and enabling the inactivation of bacterial cells on the membrane surface.

3.3. Sustainability of the sonochemical functionalization Process

The sustainability of the sonochemical process was evaluated in two different steps. First, the by-product or unbound AgMOF nanoparticles were collected to investigate their antibacterial properties. Figs. 8a–b shows the disc inhibition zone tests of the control disc with AgMOF-doped samples. As it can be seen, the by-product AgMOFs inhibited their surroundings against both *E. coli* and *S. aureus* bacteria to prove their robust antibacterial property. The TEM image of the by-product AgMOF is shown in Fig. 8c, which agrees with the typical nanosized AgMOF structure. This would candidate these AgMOF nanoparticles for other applications such as drug delivery and adsorption as investigated in previous studies [110–112].

The release rate of silver ions from the AgMOF-functionalized membranes would reflect the long-term efficacy of grafted AgMOF nanoparticles for bacterial inactivation [44,113]. Therefore, in the second step for sustainability evaluation, we analyzed the silver release via batch experiment for 14 days and the result is presented in Fig. 8d. The early silver ion release from a MOF-PDA membrane coupon (6 cm^2) was about 0.6 mg/L which rapidly decreased to around 0.2 and 0.04 mg/L, respectively, on day 3 and 4, and it started to level out at ~0.03 mg/L from day 7 on. This steady ion leaching at a relatively low rate of ~0.03 mg/L per day suggests that the membrane possesses prolonged antibacterial activities and is expected to sustainably decelerate the development of biofilms in long-term operations as well [24]. However, due to the larger pore size and surface area of the microfiltration membrane, the Ag^+ release in this work is relatively higher than in some other studies [41,114–116]. Here, the AgMOF nanoparticles can more penetrate through the larger pores of microfiltration membranes than ultrafiltration, nanofiltration, and reverse osmosis membranes used in other studies. Therefore, more AgMOFs were adsorbed on the greater surface area of the microfiltration membrane and increased the Ag^+ release.

Conclusion

A novel method was proposed to graft AgMOF nanoparticles on the surface of PVDF microfiltration membranes to improve static and dynamic antibacterial activities. First, the adhesive layer of dopamine was polymerized on the PVDF membrane surface via a simple dip-coating procedure. Then AgMOF was grown and bound to the surface of PDA-coated membranes via a facile and environmentally friendly ultrasonic-assisted technique. Morphological and chemical characterizations revealed that the AgMOFs are successfully grafted to the modified membrane's surface. Using ultra-assisted technique causes uniform and size-controlled dispersion of AgMOFs, unlike the conventional approaches with large clusters on the membrane surface. In addition, unbounded AgMOFs with high antibacterial properties can be collected and used in other applications such as drug delivery and adsorption, showing the sustainability of this technique. The static antibacterial tests showed that the antibacterial efficiency of the AgMOF-functionalized membrane was improved up to 97% compared to the pristine PVDF membrane. The dynamic biofouling experiments also revealed that the flux could be sustained by suppressing biofilm development by an AgMOF-functionalized membrane. The outstanding performance of AgMOF-functionalized membranes in static antibacterial and dynamic biofouling tests reveal the great

potential of easily implemented ultrasonic-assisted procedure for surface modification of membranes. Applying this approach to various polymeric membranes (i.e. different materials such as polysulfone and polyethersolphone) and/or feed solutions (e.g. different microorganisms) in further studies can give us more insight into different variables that could play a role in synthesis and performance of the membranes for different filtration purposes.

Data availability

Data is available on request from the authors.

Credit authorship contribution statement

Ehsan Zolghadr: Data curation, Formal analysis, Investigation, Visualization, Writing – original draft. **Mostafa Dadashi Firouzjaei**: Data curation, Formal analysis, Investigation, Visualization, Conceptualization, Project administration, Supervision, Writing – review & editing. **Sadegh Aghapour Aktij**: Data curation, Formal analysis, Investigation. **Amir Aghaei**: Formal analysis, Investigation, Writing – original draft. **Evan K. Wujcik**: Validation, Resources, Writing – review & editing. **Mohtada Sadrzadeh**: Validation, Resources, Writing – review & editing. **Ahmad Rahimpour**: Validation, Resources, Writing – review & editing. **Farhad Akbari Afkhami**: Data curation, Validation, Writing – review & editing. **Patrick LeClair**: Conceptualization, Funding acquisition, Project administration, Resources, Supervision, Writing – review & editing, **Mark Elliott**: Data curation, Formal analysis, Investigation, Visualization, Conceptualization, Project administration, Supervision, Writing – review & editing.

Declaration of competing interest

The authors declare that they have no known competing financial interests or personal relationships that could have appeared to influence the work reported in this paper.

Acknowledgment

This research benefitted greatly from funding provided by USDA TAT-RWTS 00–69526. This paper has not been formally reviewed by USDA and the views expressed in this document are solely those of the authors and do not necessarily reflect those of USDA. USDA does not endorse any products or commercial services mentioned in this publication. USDA had no role in the study design, data collection and analysis, decision to publish or preparation of the manuscript.

Appendix A. Supplementary data

Supplementary data to this article can be found online at https://doi.org/10.1016/j.mtchem.2022.101044.

References

[1] T. Carroll, S. King, S.R. Gray, B.A. Bolto, N.A. Booker, The fouling of microfiltration membranes by NOM after coagulation treatment, Water Res. 34 (2000) 2861–2868.
[2] B. Wu, S.R. Suwarno, H.S. Tan, L.H. Kim, F. Hochstrasser, T.H. Chong, M. Burkhardt, W. Pronk, A.G. Fane, Gravity-driven microfiltration pretreatment for reverse osmosis (RO) seawater desalination: microbial community characterization and RO performance, Desalination 418 (2017) 1–8.
[3] M.D. Firouzjaei, A.A. Shamsabadi, M. Sharifian Gh, A. Rahimpour, M. Soroush, A novel nanocomposite with superior antibacterial activity: a silver-based metal organic framework embellished with graphene oxide, Adv. Mater. Interfac. 5 (2018), 1701365, https://doi.org/10.1002/admi.201701365.
[4] M.A. Shannon, P.W. Bohn, M. Elimelech, J.G. Georgiadis, B.J. Marinas, A.M. Mayes, Science and technology for water purification in the coming decades, Nanosci. Technol. a Collect. Rev. from Nat. Journals. (2010) 337–346.
[5] L. Han, C. Chen, L. Shen, H. Lin, B. Li, Z. Huang, Y. Xu, R. Li, H. Hong, Novel membranes with extremely high permeability fabricated by 3D printing and nickel coating for oil/water separation, J. Mater. Chem. 10 (2022) 12055–12061.
[6] X. Zhang, Z. Wang, C.Y. Tang, J. Ma, M. Liu, M. Ping, M. Chen, Z. Wu, Modification of microfiltration membranes by alkoxysilane polycondensation induced quaternary ammonium compounds grafting for biofouling mitigation, J. Membr. Sci. 549 (2018) 165–172.
[7] H.-C. Flemming, G. Schaule, T. Griebe, J. Schmitt, A. Tamachkiarowa, Biofouling—the Achilles heel of membrane processes, Desalination 113 (1997) 215–225.
[8] P. Karami, S.A. Aktij, B. Khorshidi, M.D. Firouzjaei, A. Asad, M. Elliott, A. Rahimpour, J.B.P. Soares, M. Sadrzadeh, Nanodiamond-decorated thin film composite membranes with antifouling and antibacterial properties, Desalination 522 (2022), 115436.
[9] L. Zhang, X. Shi, M. Sun, C.J. Porter, X. Zhou, M. Elimelech, Precisely engineered photoreactive titanium nanoarray coating to mitigate biofouling in ultrafiltration, ACS Appl. Mater. Interfaces 13 (2021) 9975–9984.
[10] N. Bazrafshan, M.D. Firouzjaei, M. Elliott, A. Moradkhani, A. Rahimpour, Preparation and modification of low-fouling ultrafiltration membranes for cheese whey treatment by membrane bioreactor, Case Stud. Chem. Environ. Eng. 4 (2021), 100137.
[11] M. Li, J.C. Bradley, A.R. Badireddy, H. Lu, Ultrafiltration membranes functionalized with lipophilic bismuth dimercaptopropanol nanoparticles: antifouling behavior and mechanisms, Chem. Eng. J. 313 (2017) 293–300.
[12] J.S. Vrouwenvelder, J.C. Kruithof, M.C.M. Van Loosdrecht, Integrated approach for biofouling control, Water Sci. Technol. 62 (2010) 2477–2490.
[13] M. Ben-Sasson, X. Lu, E. Bar-Zeev, K.R. Zodrow, S. Nejati, G. Qi, E.P. Giannelis, M. Elimelech, In situ formation of silver nanoparticles on thin-film composite reverse osmosis membranes for biofouling mitigation, Water Res. 62 (2014) 260–270.
[14] K. Lee, S. Lee, S.H. Lee, S.-R. Kim, H.-S. Oh, P.-K. Park, K.-H. Choo, Y.-W. Kim, J.-K. Lee, C.-H. Lee, Fungal quorum quenching: a paradigm shift for energy savings in membrane bioreactor (MBR) for wastewater treatment, Environ. Sci. Technol. 50 (2016) 10914–10922.
[15] M. Dadashi Firouzjaei, M. Karimiziarani, H. Moradkhani, M. Elliott, B. Anasori, MXenes: the two-dimensional influencers, Mater, Today Adv 13 (2022), 100202, https://doi.org/10.1016/j.mtadv.2021.100202.
[16] V. Kochkodan, N. Hilal, A comprehensive review on surface modified polymer membranes for biofouling mitigation, Desalination 356 (2015) 187–207.
[17] B. Díez, R. Rosal, A critical review of membrane modification techniques for fouling and biofouling control in pressure-driven membrane processes, Nanotechnol. Environ. Eng. 5 (2020) 1–21.
[18] A.J.C. Semião, O. Habimana, H. Cao, R. Heffernan, A. Safari, E. Casey, The importance of laboratory water quality for studying initial bacterial adhesion during NF filtration processes, Water Res. 47 (2013) 2909–2920.
[19] C. Liu, J. Lee, J. Ma, M. Elimelech, Antifouling thin-film composite membranes by controlled architecture of zwitterionic polymer brush layer, Environ. Sci. Technol. 51 (2017) 2161–2169.
[20] Y. Liu, L. Shen, Z. Huang, J. Liu, Y. Xu, R. Li, M. Zhang, H. Hong, H. Lin, A novel in-situ micro-aeration functional membrane with excellent decoloration efficiency and antifouling performance, J. Membr. Sci. 641 (2022) 119925, https://doi.org/10.1016/J.MEMSCI.2021.119925.
[21] M. Herzberg, S. Kang, M. Elimelech, Role of extracellular polymeric substances (EPS) in biofouling of reverse osmosis membranes, Environ. Sci. Technol. 43 (2009) 4393–4398.
[22] W. Zhang, D. Guo, Z. Li, L. Shen, R. Li, M. Zhang, Y. Jiao, Y. Xu, H. Lin, A new strategy to accelerate co-deposition of plant polyphenol and amine for fabrication of antibacterial nanofiltration membranes by in-situ grown Ag nanoparticles, Separ. Purif. Technol. 280 (2022) 119866, https://doi.org/10.1016/J.SEPPUR.2021.119866.
[23] W. Zhang, W. Cheng, E. Ziemann, A. Be'er, X. Lu, M. Elimelech, R. Bernstein, Functionalization of ultrafiltration membrane with polyampholyte hydrogel and graphene oxide to achieve dual antifouling and antibacterial properties, J. Membr. Sci. 565 (2018) 293–302.
[24] J. Yin, Y. Yang, Z. Hu, B. Deng, Attachment of silver nanoparticles (AgNPs) onto thin-film composite (TFC) membranes through covalent bonding to reduce membrane biofouling, J. Membr. Sci. 441 (2013) 73–82.
[25] M. Ben-Sasson, K.R. Zodrow, Q. Genggeng, Y. Kang, E.P. Giannelis, M. Elimelech, Surface functionalization of thin-film composite membranes with copper nanoparticles for antimicrobial surface properties, Environ. Sci. Technol. 48 (2014) 384–393.
[26] M. Mozafari, S.F. Seyedpour, S.K. Salestan, A. Rahimpour, A.A. Shamsabadi, M.D. Firouzjaei, M.R. Esfahani, A. Tiraferri, H. Mohsenian, M. Sangermano, Facile Cu-BTC surface modification of thin chitosan film coated polyethersulfone membranes with improved antifouling properties for sustainable removal of manganese, J. Membr. Sci. 588 (2019), 117200.
[27] W. Cheng, X. Lu, M. Kaneda, W. Zhang, R. Bernstein, J. Ma, M. Elimelech, Graphene oxide-functionalized membranes: the importance of nanosheet surface exposure for biofouling resistance, Environ. Sci. Technol. 54 (2019) 517–526.
[28] M.S. Mauter, I. Zucker, F. Perreault, J.R. Werber, J.-H. Kim, M. Elimelech, The role of nanotechnology in tackling global water challenges, Nat. Sustain. 1 (2018) 166–175.

[29] W. Nong, J. Wu, R.A. Ghiladi, Y. Guan, The structural appeal of metal–organic frameworks in antimicrobial applications, Coord. Chem. Rev. 442 (2021), 214007.
[30] M. Berchel, T. Le Gall, C. Denis, S. Le Hir, F. Quentel, C. Elléouet, T. Montier, J.-M. Rueff, J.-Y. Salaün, J.-P. Haelters, A silver-based metal–organic framework material as a 'reservoir'of bactericidal metal ions, New J. Chem. 35 (2011) 1000–1003.
[31] A. Zirehpour, A. Rahimpour, S. Khoshhal, M.D. Firouzjaei, A.A. Ghoreyshi, The impact of MOF feasibility to improve the desalination performance and antifouling properties of FO membranes, RSC Adv. 6 (2016) 70174–70185.
[32] M. Shen, F. Forghani, X. Kong, D. Liu, X. Ye, S. Chen, T. Ding, Antibacterial applications of metal–organic frameworks and their composites, Compr. Rev. Food Sci. Food Saf. 19 (2020) 1397–1419.
[33] M.D. Firouzjaei, S.F. Seyedpour, S.A. Aktij, M. Giagnorio, N. Bazrafshan, A. Mollahosseini, F. Samadi, S. Ahmadalipour, F.D. Firouzjaei, M.R. Esfahani, Recent advances in functionalized polymer membranes for biofouling control and mitigation in forward osmosis, J. Membr. Sci. 596 (2020), 117604.
[34] Y. Xiao, W. Zhang, Y. Jiao, Y. Xu, H. Lin, Metal-phenolic network as precursor for fabrication of metal-organic framework (MOF) nanofiltration membrane for efficient desalination, J. Membr. Sci. 624 (2021), 119101.
[35] S.M. Nejad, S.F. Seyedpour, S.A. Aktij, M.D. Firouzjaei, M. Elliott, A. Tiraferri, M. Sadrzadeh, A. Rahimpour, Loose nanofiltration membranes functionalized with in situ-synthesized metal organic framework for water treatment, Mater. Today Chem. 24 (2022), 100909.
[36] J. Liu, L. Shen, H. Lin, Z. Huang, H. Hong, C. Chen, Preparation of Ni@UiO-66 incorporated polyethersulfone (PES) membrane by magnetic field assisted strategy to improve permeability and photocatalytic self-cleaning ability, J. Colloid Interface Sci. 618 (2022) 483–495, https://doi.org/10.1016/J.JCIS.2022.03.106.
[37] Y. Xu, Y. Xiao, W. Zhang, H. Lin, L. Shen, R. Li, Y. Jiao, B.Q. Liao, Plant polyphenol intermediated metal-organic framework (MOF) membranes for efficient desalination, J. Membr. Sci. 618 (2021), 118726, https://doi.org/10.1016/J.MEMSCI.2020.118726.
[38] W. Zhang, Z. Li, Y. Xu, H. Lin, L. Shen, R. Li, M. Zhang, In situ conversion of ZnO into zeolitic imidazolate framework-8 in polyamide layers for well-structured high-permeance thin-film nanocomposite nanofiltration membranes, J. Mater. Chem. A. 9 (2021) 7684–7691, https://doi.org/10.1039/D0TA11923G.
[39] Z. Li, W. Zhang, M. Tao, L. Shen, R. Li, M. Zhang, Y. Jiao, H. Hong, Y. Xu, H. Lin, In-situ growth of UiO-66-NH2 in porous polymeric substrates at room temperature for fabrication of mixed matrix membranes with fast molecular separation performance, Chem. Eng. J. 435 (2022), 134804, https://doi.org/10.1016/J.CEJ.2022.134804.
[40] M. Pejman, M.D. Firouzjaei, S.A. Aktij, P. Das, E. Zolghadr, H. Jafarian, A.A. Shamsabadi, M. Elliott, M.R. Esfahani, M. Sangermano, Improved anti-fouling and antibacterial properties of forward osmosis membranes through surface modification with zwitterions and silver-based metal organic frameworks, J. Membr. Sci. (2020), 118352.
[41] M. Pejman, M. Dadashi Firouzjaei, S. Aghapour Aktij, P. Das, E. Zolghadr, H. Jafarian, A. Arabi Shamsabadi, M. Elliott, M. Sadrzadeh, M. Sangermano, In situ Ag-MOF growth on pre-grafted zwitterions imparts outstanding anti-fouling properties to forward osmosis membranes, ACS Appl. Mater. Interfaces 12 (2020) 36287–36300.
[42] K. Martin-Betancor, S. Aguado, I. Rodea-Palomares, M. Tamayo-Belda, F. Leganes, R. Rosal, F. Fernandez-Pinas, Co, Zn and Ag-MOFs evaluation as biocidal materials towards photosynthetic organisms, Sci. Total Environ. 595 (2017) 547–555.
[43] W. Xu, H. Zhuang, Z. Xu, M. Huang, S. Gao, Q. Li, G. Zhang, Design and construction of Ag@ MOFs immobilized PVDF ultrafiltration membranes with anti-bacterial and antifouling properties, Adv. Polym. Technol. 2020 (2020).
[44] M.D. Firouzjaei, M. Pejman, M.S. Gh, S.A. Aktij, E. Zolghadr, A. Rahimpour, M. Sadrzadeh, A.A. Shamsabadi, A. Tiraferri, M. Elliott, Functionalized polyamide membranes yield suppression of biofilm and planktonic bacteria while retaining flux and selectivity, Separ. Purif. Technol. (2021), 119981.
[45] A. Aghaei, M. Dadashi Firouzjaei, P. Karami, S.A. Aktij, M. Elliott, Y. Mansourpanah, A. Rahimpour, J. Soares, M. Sadrzadeh, The implications of 3D-printed membranes for water and wastewater treatment and resource recovery, Can. J. Chem. Eng. (2022).
[46] N. Stock, S. Biswas, Synthesis of metal-organic frameworks (MOFs): routes to various MOF topologies, morphologies, and composites, Chem. Rev. 112 (2012) 933–969.
[47] Y.-R. Lee, J. Kim, W.-S. Ahn, Synthesis of metal-organic frameworks: a mini review, Korean J. Chem. Eng. 30 (2013) 1667–1680.
[48] Y. Bian, N. Xiong, G. Zhu, Technology for the remediation of water pollution: a review on the fabrication of metal organic frameworks, Processes 6 (2018) 122.
[49] E. Zolghadr, M.D. Firouzjaei, G. Amouzandeh, P. LeClair, M. Elliott, The role of membrane-based technologies in environmental treatment and reuse of produced water, Front. Environ. Sci. 9 (2021) 71.
[50] G. Chatel, How sonochemistry contributes to green chemistry? Ultrason. Sonochem. 40 (2018) 117–122.
[51] J.-L. Luche, Synthetic Organic Sonochemistry, Springer Science & Business Media, 2013.
[52] J.H. Bang, K.S. Suslick, Applications of ultrasound to the synthesis of nanostructured materials, Adv. Mater. 22 (2010) 1039–1059.
[53] M. Dadashi Firouzjaei, E. Zolghadr, S. Ahmadalipour, N. Taghvaei, F. Akbari Afkhami, S. Nejati, M.A. Elliott, Chemistry, abundance, detection and treatment of per-and polyfluoroalkyl substances in water: a review, Environ. Chem. Lett. (2021) 1–19.
[54] W.-J. Son, J. Kim, J. Kim, W.-S. Ahn, Sonochemical synthesis of MOF-5, Chem. Commun. (2008) 6336–6338.
[55] J. Jiang, L. Zhu, L. Zhu, B. Zhu, Y. Xu, Surface characteristics of a self-polymerized dopamine coating deposited on hydrophobic polymer films, Langmuir 27 (2011) 14180–14187.
[56] P. Zhou, Y. Deng, B. Lyu, R. Zhang, H. Zhang, H. Ma, Y. Lyu, S. Wei, Rapidly-deposited polydopamine coating via high temperature and vigorous stirring: formation, characterization and biofunctional evaluation, PLoS One 9 (2014), e113087.
[57] R. Zhang, Y. Xu, L. Shen, R. Li, H. Lin, Preparation of nickel@polyvinyl alcohol (PVA) conductive membranes to couple a novel electrocoagulation-membrane separation system for efficient oil-water separation, J. Membr. Sci. 653 (2022), 120541, https://doi.org/10.1016/J.MEMSCI.2022.120541.
[58] L. Rao, X. You, B. Chen, L. Shen, Y. Xu, M. Zhang, H. Hong, R. Li, H. Lin, A novel composite membrane for simultaneous separation and catalytic degradation of oil/water emulsion with high performance, Chemosphere 288 (2022), 132490, https://doi.org/10.1016/J.CHEMOSPHERE.2021.132490.
[59] B. Chen, X. Hu, J. Wang, R. Li, L. Shen, Y. Xu, M. Zhang, H. Hong, H. Lin, Novel catalytic self-cleaning membrane with peroxymonosulfate activation for dual-function wastewater purification: performance and mechanism, J. Clean. Prod. 355 (2022), 131858, https://doi.org/10.1016/J.JCLEPRO.2022.131858.
[60] C. Liu, A.F. Faria, J. Ma, M. Elimelech, Mitigation of biofilm development on thin-film composite membranes functionalized with zwitterionic polymers and silver nanoparticles, Environ. Sci. Technol. 51 (2017) 182–191.
[61] M. Pejman, M.D. Firouzjaei, S.A. Aktij, E. Zolghadr, P. Das, M. Elliott, M. Sadrzadeh, M. Sangermano, A. Rahimpour, A. Tiraferri, Effective strategy for UV-mediated grafting of biocidal Ag-MOFs on polymeric membranes aimed at enhanced water ultrafiltration, Chem. Eng. J. (2021), 130704.
[62] Y. Hu, H. Yang, R. Wang, M. Duan, Fabricating Ag@ MOF-5 nanoplates by the template of MOF-5 and evaluating its antibacterial activity, Colloids Surfaces A Physicochem. Eng. Asp. 626 (2021), 127093.
[63] X. Lu, Y. Peng, L. Ge, R. Lin, Z. Zhu, S. Liu, Amphiphobic PVDF composite membranes for anti-fouling direct contact membrane distillation, J. Membr. Sci. 505 (2016) 61–69.
[64] S. Mohamadi, Preparation and characterization of PVDF/PMMA/graphene polymer blend nanocomposites by using ATR-FTIR technique, Infrared Spectrosc. Sci. Eng. Technol. 1 (2012).
[65] M. Ulaganathan, S. Rajendran, Preparation and characterizations of PVAc/P(VdF-HFP)-based polymer blend electrolytes, Ionics 16 (2010) 515–521.
[66] W. Ma, H. Yuan, X. Wang, The effect of chain structures on the crystallization behavior and membrane formation of poly (vinylidene fluoride) copolymers, Membranes 4 (2014) 243–256.
[67] P. Martins, A.C. Lopes, S. Lanceros-Mendez, Electroactive phases of poly (vinylidene fluoride): determination, processing and applications, Prog. Polym. Sci. 39 (2014) 683–706.
[68] N. Betz, A. Le Moël, E. Balanzat, J.M. Ramillon, J. Lamotte, J.P. Gallas, G. Jaskierowicz, A FTIR study of PVDF irradiated by means of swift heavy ions, J. Polym. Sci., Part B: Polym. Phys. 32 (1994) 1493–1502.
[69] A. Jabbarnia, R. Asmatulu, Synthesis and characterization of PVdF/PVP-based electrospun membranes as separators for supercapacitor applications, J. Mater. Sci. Technol. Res. 2 (2015) 43–51.
[70] H. Wu, J.M. Ang, J. Kong, C. Zhao, Y. Du, X. Lu, One-pot synthesis of polydopamine–Zn complex antifouling coatings on membranes for ultrafiltration under harsh conditions, RSC Adv. 6 (2016) 103390–103398.
[71] H. Luo, C. Gu, W. Zheng, F. Dai, X. Wang, Z. Zheng, Facile synthesis of novel size-controlled antibacterial hybrid spheres using silver nanoparticles loaded with poly-dopamine spheres, RSC Adv. 5 (2015) 13470–13477.
[72] S.K. Mahadeva, J. Berring, K. Walus, B. Stoeber, Effect of poling time and grid voltage on phase transition and piezoelectricity of poly (vinyledene fluoride) thin films using corona poling, J. Phys. D Appl. Phys. 46 (2013), 285305.
[73] N. Kaur, J. Bahadur, V. Panwar, P. Singh, K. Rathi, K. Pal, Effective energy harvesting from a single electrode based triboelectric nanogenerator, Sci. Rep. 6 (2016) 1–9.
[74] S.F. Seyedpour, A. Arabi Shamsabadi, S. Khoshhal Salestan, M. Dadashi Firouzjaei, M. Sharifian Gh, A. Rahimpour, F. Akbari Afkhami, M. reza Shirzad Kebria, M.A. Elliott, A. Tiraferri, Tailoring the biocidal activity of novel silver-based metal Azolate frameworks, ACS Sustain. Chem. Eng. 8 (20) (2020) 7588–7599.
[75] Y. Meng, A sustainable approach to fabricating Ag nanoparticles/PVA hybrid nanofiber and its catalytic activity, Nanomaterials 5 (2015) 1124–1135.
[76] H. Guo, Y. Zhang, Z. Zheng, H. Lin, Y. Zhang, Facile one-pot fabrication of Ag@ MOF (Ag) nanocomposites for highly selective detection of 2, 4, 6-trinitrophenol in aqueous phase, Talanta 170 (2017) 146–151.
[77] J. Liu, D.M. Strachan, P.K. Thallapally, Enhanced noble gas adsorption in Ag@ MOF-74Ni, Chem. Commun. 50 (2014) 466–468.
[78] P. Viswanath, M. Yoshimura, Light-induced reversible phase transition in polyvinylidene fluoride-based nanocomposites, SN Appl. Sci. 1 (2019) 1–9.
[79] M.T. Riosbaas, K.J. Loh, G. O'Bryan, B.R. Loyola, In situ phase change characterization of PVDF thin films using Raman spectroscopy, in: Sensors Smart Struct. Technol. Civil, Mech. Aerosp. Syst., International Society for Optics and Photonics, 2014, p. 90610Z, 2014.

[80] J. Ma, Q. Zhang, K. Lin, L. Zhou, Z. Ni, Piezoelectric and optoelectronic properties of electrospinning hybrid PVDF and ZnO nanofibers, Mater. Res. Express 5 (2018), 35057.
[81] I.S. Elashmawi, L.H. Gaabour, Raman, morphology and electrical behavior of nanocomposites based on PEO/PVDF with multi-walled carbon nanotubes, Results Phys. 5 (2015) 105–110.
[82] J.D. Ciubuc, C. Qiu, K.E. Bennet, M. Alonzo, W. Durrer, F.S. Manciu, Raman computational and experimental studies of dopamine molecules on silver nanocolloids, in: 2017 IEEE Int. Symp. Med. Meas. Appl., IEEE, 2017, pp. 153–158.
[83] Y. Bai, Z. Yu, R. Liu, N. Li, S. Yan, K. Yang, B. Liu, D. Wei, L. Wang, Pressure-induced crystallization and phase transformation of para-xylene, Sci. Rep. 7 (2017) 1–10.
[84] D. Jiang, A. Urakawa, M. Yulikov, T. Mallat, G. Jeschke, A. Baiker, Size selectivity of a copper metal–organic framework and origin of catalytic activity in epoxide alcoholysis, Chem. Eur J. 15 (2009) 12255–12262.
[85] X. Zhang, Q. Zhou, Y. Huang, Z. Li, Z. Zhang, Contrastive analysis of the Raman spectra of polychlorinated benzene: hexachlorobenzene and benzene, Sensors 11 (2011) 11510–11515.
[86] Y. Zhu, J. Wang, F. Zhang, S. Gao, A. Wang, W. Fang, J. Jin, Zwitterionic nanohydrogel grafted PVDF membranes with comprehensive antifouling property and superior cycle stability for oil-in-water emulsion separation, Adv. Funct. Mater. 28 (2018), 1804121.
[87] L. Ying, P. Wang, E.T. Kang, K.G. Neoh, Synthesis and characterization of poly (acrylic acid)-graft-poly (vinylidene fluoride) copolymers and pH-sensitive membranes, Macromolecules 35 (2002) 673–679.
[88] M. Mohammadi Ghaleni, A. Al Balushi, S. Kaviani, E. Tavakoli, M. Bavarian, S. Nejati, Fabrication of Janus membranes for desalination of oil-contaminated saline water, ACS Appl. Mater. Interfaces 10 (2018) 44871–44879.
[89] T.L. Barr, S. Seal, Nature of the use of adventitious carbon as a binding energy standard, J. Vac. Sci. Technol. A Vacuum, Surfaces, Film. 13 (1995) 1239–1246.
[90] J. Gomez-Bolivar, I.P. Mikheenko, R.L. Orozco, S. Sharma, D. Banerjee, M. Walker, R.A. Hand, M.L. Merroun, L.E. Macaskie, Synthesis of Pd/Ru bimetallic nanoparticles by Escherichia coli and potential as a catalyst for upgrading 5-hydroxymethyl furfural into liquid fuel precursors, Front. Microbiol. 10 (2019) 1276.
[91] S.F. Seyedpour, M. Dadashi Firouzjaei, A. Rahimpour, E. Zolghadr, A. Arabi Shamsabadi, P. Das, F. Akbari Afkhami, M. Sadrzadeh, A. Tiraferri, M.A. Elliott, Toward sustainable tackling of biofouling implications and improved performance of TFC FO membranes modified by Ag-MOFs nanorods, ACS Appl. Mater. Interfaces 12 (34) (2020) 38285–38298.
[92] F.R.A. dos Santos, C.P. Borges, F.V. da Fonseca, Polymeric materials for membrane contactor devices applied to water treatment by ozonation, Mater. Res. 18 (2015) 1015–1022.
[93] M. Tao, F. Liu, L. Xue, Hydrophilic poly (vinylidene fluoride)(PVDF) membrane by in situ polymerisation of 2-hydroxyethyl methacrylate (HEMA) and micro-phase separation, J. Mater. Chem. 22 (2012) 9131–9137.
[94] G. Liu, J. Xiang, Q. Xia, K. Li, H. Yan, L. Yu, Fabrication of durably antibacterial cotton fabrics by robust and uniform immobilization of silver nanoparticles via mussel-inspired polydopamine/polyethyleneimine coating, Ind. Eng. Chem. Res. 59 (2020) 9666–9678.
[95] C. Shang, D. Pranantyo, S. Zhang, Understanding the roughness–fouling relationship in reverse osmosis: mechanism and implications, Environ. Sci. Technol. 54 (2020) 5288–5296.
[96] G.Z. Ramon, E.M.V. Hoek, Transport through composite membranes, part 2: impacts of roughness on permeability and fouling, J. Membr. Sci. 425 (2013) 141–148.
[97] G. Xue, Y. Zhang, T. Xie, Z. Zhang, Q. Liu, X. Li, X. Gou, Cell adhesion-mediated piezoelectric self-stimulation on polydopamine-modified poly (vinylidene fluoride) membranes, ACS Appl. Mater. Interfaces 13 (2021) 17361–17371.
[98] H. Zheng, D. Wang, X. Sun, S. Jiang, Y. Liu, D. Zhang, L. Zhang, Surface modified by green synthetic of Cu-MOF-74 to improve the anti-biofouling properties of PVDF membranes, Chem. Eng. J. 411 (2021), 128524.
[99] A. Rahimpour, S.F. Seyedpour, S. Aghapour Aktij, M. Dadashi Firouzjaei, A. Zirehpour, A. Arabi Shamsabadi, S. Khoshhal Salestan, M. Jabbari, M. Soroush, Simultaneous improvement of antimicrobial, antifouling, and transport properties of forward osmosis membranes with immobilized highly-compatible polyrhodanine nanoparticles, Environ. Sci. Technol. 52 (9) (2018) 5246–5258.
[100] C. Xu, W. Chen, H. Gao, X. Xie, Y. Chen, Cellulose nanocrystal/silver (CNC/Ag) thin-film nanocomposite nanofiltration membranes with multifunctional properties, Environ. Sci. Nano. 7 (2020) 803–816.
[101] D. Johnson, N. Hilal, Characterisation and quantification of membrane surface properties using atomic force microscopy: a comprehensive review, Desalination 356 (2015) 149–164.
[102] M.M.A. Shirazi, A. Kargari, S. Bazgir, M. Tabatabaei, M.J.A. Shirazi, M.S. Abdullah, T. Matsuura, A.F. Ismail, Characterization of electrospun polystyrene membrane for treatment of biodiesel's water-washing effluent using atomic force microscopy, Desalination 329 (2013) 1–8.
[103] A. Lindholdt, K. Dam-Johansen, S.M. Olsen, D.M. Yebra, S. Kiil, Effects of biofouling development on drag forces of hull coatings for ocean-going ships: a review, J. Coating Technol. Res. 12 (2015) 415–444.
[104] L. Su, Y. Yu, Y. Zhao, F. Liang, X. Zhang, Strong antibacterial polydopamine coatings prepared by a shaking-assisted method, Sci. Rep. 6 (2016) 1–8.
[105] N.A. Travlou, M. Algarra, C. Alcoholado, M. Cifuentes-Rueda, A.M. Labella, J.M. Lázaro-Martínez, E. Rodríguez-Castellón, T.J. Bandosz, Carbon quantum dot surface-chemistry-dependent Ag release governs the high antibacterial activity of Ag-metal–organic framework composites, ACS Appl. Bio Mater. 1 (2018) 693–707.
[106] J. Zhang, S. Li, W. Wang, J. Pei, J. Zhang, T. Yue, W. Youravong, Z. Li, Bacteriocin assisted food functional membrane for simultaneous exclusion and inactivation of Alicyclobacillus acidoterrestris in apple juice, J. Membr. Sci. 618 (2021), 118741.
[107] R. Sonohara, N. Muramatsu, H. Ohshima, T. Kondo, Difference in surface properties between Escherichia coli and Staphylococcus aureus as revealed by electrophoretic mobility measurements, Biophys. Chem. 55 (1995) 273–277.
[108] M. Riley, Correlates of smallest sizes for microorganisms, in: Size Limits Very Small Microorg. Proc. a Work.,, 1999, p. 21.
[109] A.M. Madsen, I. Kurdi, L. Feld, K. Tendal, Airborne MRSA and total Staphylococcus aureus as associated with particles of different sizes on Pig Farms, Ann. Work Expo. Heal. 62 (2018) 966–977.
[110] S. Mallakpour, E. Nikkhoo, C.M. Hussain, Application of MOF materials as drug delivery systems for cancer therapy and dermal treatment, Coord. Chem. Rev. 451 (2022), 214262.
[111] M.D. Firouzjaei, A.A. Shamsabadi, M.S. Gh, A. Rahimpour, M. Soroush, A novel nanocomposite with superior antibacterial activity: a silver-based metal organic framework embellished with graphene oxide, Adv. Mater. Interfac. 5 (11) (2018), 1701365.
[112] M. Dadashi Firouzjaei, F. Akbari Afkhami, M. Rabbani Esfahani, C.H. Turner, S. Nejati, Experimental and molecular dynamics study on dye removal from water by a graphene oxide-copper-metal organic framework nanocomposite, J. Water Proc. Eng. 34 (2020), 101180, https://doi.org/10.1016/j.jwpe.2020.101180.
[113] M.S. Mauter, Y. Wang, K.C. Okemgbo, C.O. Osuji, E.P. Giannelis, M. Elimelech, Antifouling ultrafiltration membranes via post-fabrication grafting of biocidal nanomaterials, ACS Appl. Mater. Interfaces 3 (2011) 2861–2868.
[114] Z.K. Tan, J.L. Gong, S.Y. Fang, J. Li, W.C. Cao, Z.P. Chen, Outstanding antibacterial thin-film composite membrane prepared by incorporating silver-based metal–organic framework (Ag-MOF) for water treatment, Appl. Surf. Sci. 590 (2022), 153059, https://doi.org/10.1016/J.APSUSC.2022.153059.
[115] A. Zirehpour, A. Rahimpour, A. Arabi Shamsabadi, M.G. Sharifian, M. Soroush, Mitigation of thin-film composite membrane biofouling via immobilizing nano-sized biocidal reservoirs in the membrane active layer, Environ. Sci. Technol. 51 (2017) 5511–5522, https://doi.org/10.1021/ACS.EST.7B00782/SUPPL_FILE/ES7B00782_SI_001.PDF.
[116] M.D. Firouzjaei, A.A. Shamsabadi, S.A. Aktij, S.F. Seyedpour, M. Sharifian Gh, A. Rahimpour, M.R. Esfahani, M. Ulbricht, M. Soroush, Exploiting synergetic effects of graphene oxide and a silver-based metal–organic framework to enhance antifouling and anti-biofouling properties of thin-film nanocomposite membranes, ACS Appl. Mater. Interfaces 10 (2018) 42967–42978.